EPJ manuscript No.
(will be inserted by the editor)

Lattice Boltzmann simulations of capillary filling: finite vapour density effects

Lattice boltzmann simulations of capillary filling

F. Diotallevi[1], L.Biferale[2], S. Chibbaro[3], G. Pontrelli[1], F. Toschi[1], and S. Succi[1]

[1] Istituto per le Applicazioni del Calcolo CNR, Viale del Policlinico 137, 00161 Roma, Italy.
[2] Dept. of Physics and INFN, University of Tor Vergata, Via della Ricerca Scientifica 1, 00133 Roma, Italy.
[3] Dept. of Mechanical Engineering, University of Tor Vergata, Viale Politecnico 8, Rome, Italy.

Received: date / Revised version: date

Abstract. Numerical simulations of two-dimensional capillary filling using the pseudo-potential lattice Boltzmann model for multiphase fluids are presented, with special emphasis on the role of finite-vapour density effects. It is shown that whenever the density of the light-phase exceeds about ten percent of the dense phase, the front motion proceeds through a combined effect of capillary advection and condensation. As a result, under these conditions, the front proceeds at a higher speed as compared to the Washburn prediction. It is suggested that such an acceleration effect might be observed in experiments performed sufficiently close to critical conditions.

PACS. 83.50.Rp , – 68.03.Cd

1 Introduction

In the recent years, increasing attention has been paid to the use of lattice Boltzmann (LB) techniques beyond the strictly hydrodynamic regime, i.e. for micro and nanofluidic applications. LB holds great potential for these applications because it can offer an optimal compromise between the physical realism of atomistic methods and the computational efficiency of continuum fluid mechanics. However, turning this potential into a robust and reliable prediction tool for complex micro/nanofluidic problems, requires a detailed and *quantitative* validation program on a number of test and benchmark problems. In this work, we present one such validation study, as applied to the important problem of capillary filling. Capillary filling is an old problem, originating with the pioneering works of Washburn [1] and Lucas [2]. Recently, with the explosion of theoretical, experimental and numerical works on microphysics and nanophysics, the problem attracted considerable renewed interest [3–6]. Capillary filling is a typical "moving contact line" problem, in which interface motion can only take place thanks to subtle non-hydrodynamic effects occurring at the contact point between liquid-gas and solid phase. As a result, it offers an ideal testground for assessing the capabilities of mesoscopic methods, such as LB, to describe phenomena beyond the hydrodynamic regime.

2 The Washburn description

A simple and yet powerful picture of capillary motion was developed back in 20's with the pioneering work of Washburn and Lucas. The Washburn picture is easily derived by writing the momentum equation for the mass of moving liquid in the capillary. This leads to the following equation:

$$\rho_l \frac{d}{d\tilde{t}}(\tilde{z}\dot{\tilde{z}}) = \frac{2\gamma cos(\theta)}{H} - \frac{12\mu_l \tilde{z}\dot{\tilde{z}}}{H^2} \tag{1}$$

where $\tilde{z}(t)$ is centerline position of the advancing front at time $\tilde{t}$, H the transverse size of the channel, γ is the surface tension, θ is the static contact angle, ρ_l the density and μ_l the viscosity of the liquid. The factor 12 stems from the specific geometry considered here, i.e. two infinite parallel plates separated by a distance H – see fig. 1). More precisely, in the overdamped regime, the Washburn solution reads as follows:

$$\tilde{z}^2(\tilde{t}) - \tilde{z}^2(0) = \frac{\gamma H cos(\theta)}{3\mu_l}\tilde{t} \tag{2}$$

To the purpose of comparing with experimental results, it is useful to recast this relation in dimensionless form (reduced units), $t = \tilde{t}/t_{cap}$ and $z = \tilde{z}/H$, being the capillary time $t_{cap} = H\mu/\gamma$. This leads to the universal law:

$$z^2(t) - z^2(0) = \frac{cos(\theta)}{3}t. \tag{3}$$

The Washburn solution (3) above spells troubles for microfluidic applications where fast-fill is a goal. Indeed, (3) clearly shows that the front moves at increasingly lower speed as it propagates down the capillary. The reason is easily understood by noting that, according to the eq. 1, the front position $z(t)$ evolves like the trajectory of a point-like particle, whose mass grows linearly with the position z, driven by a constant capillary force and damped by a dissipative force also growing linearly with z. By neglecting inertia (overdamped regime), the capillary force competes with a linearly increasing dissipation, which ultimately leads to a front speed $\dot{z}$ decaying like $1/z$. Strategies to do away with this basic limitation make the object of intense scientific and technological research, such as interface functionalization, optimal coating, and related issues. As already remarked in the literature [5], the asymptotic behaviour (3) hinges on a number of simplifying assumptions, namely: (i) the inertial terms in the Navier-Stokes equation are negligible, (ii) the instantaneous *bulk* profile is given by the Poiseuille flow, (iii) the microscopic slip mechanism which allows for the interface motion is not relevant for bulk quantities (such as the overall position of the interface inside the channel), (iv) inlet and outlet phenomena can be neglected (limit of infinitely long channels); (v) the liquid is filling in a capillary, either empty or filled with gas whose total mass is negligible with respect to the liquid one. None of these assumptions needs to be true in actual experiments, and to the purpose of comparison with experimental data, it is therefore important to address these limitations within a suitably generalization of the Washburn equation, to which we shall return shortly. In this paper, we shall be interested specifically in the finite-vapour density issue (v).

3 LBE for capillary filling

The model used in this work is a suitable adaptation of the Shan-Chen pseudo-potential LBE [7] with hydrophobic/hydrophilic boundaries conditions, as developed in [8, 9]. Other models with different boundary conditions and/or non-ideal interactions have been also used in [10].

The geometry is depicted in fig. (1). The bottom and top surface is coated only in the right half of the channel, with a boundary condition imposing a given static contact angle [8]; in the left half, we impose periodic boundary conditions at top and bottom surfaces, so as to realize a flat liquid-gas interface mimicking an "infinite reservoir". Periodic boundary conditions are also imposed at the two lateral sides, so as to ensure total conservation of mass inside the system.

3.1 LBE algorithm for multi-phase flows

We start from the usual lattice Boltzmann equation with a single-time relaxation [11,12]:

$$f_l(\boldsymbol{x}+\boldsymbol{c}_l\Delta t, t+\Delta t)-f_l(\boldsymbol{x},t) = -\frac{\Delta t}{\tau_B}\left(f_l(\boldsymbol{x},t) - f_l^{(eq)}(\rho,\rho\boldsymbol{u})\right) \quad (4)$$

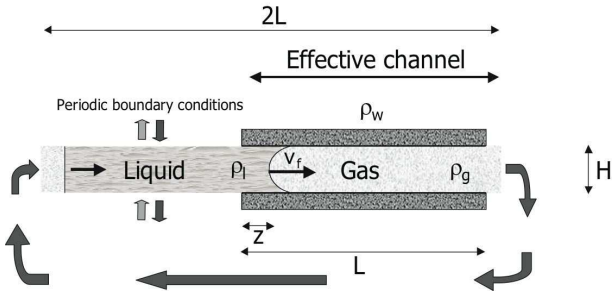

Fig. 1. Geometrical set-up of the numerical LBE. The 2 dimensional geometry, with length $2L$ and width H, is divided in two parts. The left part has top and bottom periodic boundary conditions such as to support a perfectly flat gas-liquid interface, mimicking a "infinite reservoir". In the right half, of length L, there is the true capillary: the top and bottom boundary conditions are those of a solid wall, with a given contact angle θ [8]. Periodic boundary conditions are also imposed at the west and east sides.

where $f_l(\boldsymbol{x},t)$ is the kinetic probability density function associated with a mesoscopic velocity $\boldsymbol{c}_l$, τ_B is a mean collision time (with Δt a time lapse), $f_l^{(eq)}(\rho,\rho\boldsymbol{u})$ the equilibrium distribution, corresponding to the Maxwellian distribution in the continuum limit. From the kinetic distributions we can define macroscopic density and momentum fields as [11,12]:

$$\rho(\boldsymbol{x}) = \sum_l f_l(\boldsymbol{x}); \qquad \rho\boldsymbol{u}(\boldsymbol{x}) = \sum_l \boldsymbol{c}_l f_l(\boldsymbol{x}). \quad (5)$$

For technical details and numerical simulations we shall refer to the nine-speed, two-dimensional $2DQ9$ model [11]. The equilibrium distribution in the lattice Boltzmann equations is obtained via a low Mach number expansion of the equilibrium Maxwellian [11,12]. In order to study non-ideal effects we need to supplement the previous description with an interparticle forcing. This is done by adding a suitable F_l in (4). In the original model [7], the bulk interparticle interaction is proportional to a free parameter (the ratio of potential to thermal energy), G, entering the equation for the momentum balance:

$$F_i = -Gc_s^2 \sum_l w(|\boldsymbol{c}_l|^2)\psi(\boldsymbol{x},t)\psi(\boldsymbol{x}+\boldsymbol{c}_l\Delta t,t)c_l^i \quad (6)$$

being $w(|\boldsymbol{c}_l|^2)$ the static weights for the standard case of 2DQ9 [11] and $\psi(\boldsymbol{x},t) = \psi(\rho(\boldsymbol{x},t))$ the pseudo-potential function which describes the fluid-fluid interactions triggered by inhomogeneities of the density profile (see [7–9] for details).

One may show [8,9] that the above pseudo-potential, leads to a non-ideal pressure tensor given by (upon Taylor expanding the forcing term):

$$P_{ij} = \left(c_s^2\rho + G\frac{c_s^2}{2}\psi^2 + G\frac{c_s^4}{4}|\nabla\psi|^2 + G\frac{c_s^4}{2}\psi\Delta\psi\right)\delta_{ij} - \\ - \frac{1}{2}Gc_s^4\partial_i\psi\partial_j\psi + \mathcal{O}(\partial^4), \quad (7)$$

where c_s is the sound speed. This approach allows the definition of a static contact angle θ, by means of a suitable value for the pseudo-potential $\psi_w = \psi(\rho_w)$ [8], which can span the range $\theta \in [0^o : 180^o]$. Moreover, it also defines a specific value for the surface tension, γ_{lg}, via the usual integration of the offset between normal and transverse components of the pressure tensor along the liquid-gas interface [7–9].

As to the boundary conditions on the Boltzmann populations, the standard bounce-back rule is imposed. One can show that the bounce-back rule gives no-slip boundary conditions up to second order in the Knudsen number in the hydrodynamical limit of single phase flows [14]. In the presence of strong density variations, close to the walls across the interface, the velocity parallel to the wall may develop a small slip length (of the order of the interface thickness, $\lambda_s \propto \xi$) which, in turn, allows the interface to move. At variance with continuum formulations, in which the slip length is prescribed a-priori, our mesoscopic model allows slip flow to develop on its own as a result of the fluid-wall interactions coded in the mesoscopic wall potential ψ_w. However, it is difficult to control exactly this phenomenon, because even imposing an exact no-slip boundary condition at the wall [15], the model does develop its own dynamics at the first node away from the wall, thus leading to an overall non-zero slip velocity. To the purpose of controlling the capillary filling, one may reabsorb all these effects within the usual Maxwell slip boundary conditions: $u_s = \lambda_s \partial_n u$. It is easy to show that in presence of a slip velocity, the Poiseuille profile becomes:

$$u(y) = 6\frac{\bar{u}}{H^2}\frac{y(H-y)+\lambda_s H}{1+6\lambda_s/H} \tag{8}$$

where the velocity of the front must be identified with the mean velocity, $\bar{u} \equiv 1/H \int_0^H u(y)dy = \dot{z}$. Therefore, the Washburn law (3) becomes:

$$z^2(t) - z^2(0) = A\frac{cos(\theta)}{3}t \tag{9}$$

where

$$A = 1 + 6\frac{\lambda_s}{H} \tag{10}$$

accounts for finite-slip slow effects. Under ordinary conditions, the slip length is of the same order of the atomistic interaction scale, hence $\xi/H < 10^{-3}$, so that slip-effects can be neglected to all practical purposes. This situation can drastically change in the presence of superhydrophic effects, although we shall not be concerned with these problems in the present work.

3.2 Generalized Washburn equation

As already remarked many years ago [16], the Washburn law (3) holds in the limit where inertial forces can be neglected with respect to the viscous and capillary ones. This cannot be true in the early stage of the filling process, where strong acceleration drives the interface inside the capillary. However, putting typical numbers for microfluidic devices ($H \simeq 1\mu m$, $\gamma \simeq 0.072 N/m$, $\rho_l \simeq 10^{-3} kg/m^3$, $\mu_l \simeq 10^{-3} Ns/m^2$), it is readily checked that the transient time, $\tau_{diff} = H\gamma\rho_l/\mu_l^2$, is of the order of a few nanoseconds, hence completely negligible for most practical purposes.

Another important effect which must be kept in mind when simulating capillary filling, is the unavoidable "resistance" of the gas occupying the capillary during the liquid invasion. This is a particular "sensitive" issue for LB techniques, because reaching the typical 1 : 1000 density ratio between liquid and gas of experimental set up, represents a challenge for most numerical methods, particularly for multiphase Lattice Boltzmann, typically operating in the regime 1 : 10 to 1 : 100. In order to take in to account both effects, inertia and gas dynamics, one may write down the balance between the total momentum change inside the capillary and the force (per unit width) acting on the liquid+gas system (here untilded symbols denote physical units):

$$\frac{d(\dot{z}M(t))}{dt} = F_{cap} + F_{vis} \tag{11}$$

where $M(t) = M_g + M_l$ is the total mass of liquid and gas inside the capillary at any given time. The two forces in the right hand side correspond to the capillary force, $F_{cap} = 2\gamma cos(\theta)$, and to the viscous drag $F_{vis} = -2(\mu_g(L-z) + \mu_l z)\partial_n u(0)$. Following the notation of fig.(1) and the expression for the velocity profile (8) one obtains the final expression (see also [17] for a similar derivation, without considering the slip velocity):

$$(\rho_g(L-z) + \rho_l z)\ddot{z} + (\rho_l - \rho_g)(\dot{z})^2 = 2\frac{\gamma cos(\theta)}{H} - \frac{12\dot{z}}{H^2(1+6\frac{\lambda_s}{H})}[(\mu_g(L-z) + \mu_l z)] \tag{12}$$

In the above equation for the front dynamics, the terms in the LHS take into account the fluid inertia. Being proportional either to the acceleration or to the squared velocity, they become negligible for long times. Washburn law plus the slip correction (9) is therefore correctly recovered asymptotically, for $t \to \infty$, and in the limit when $\rho_g/\rho_l \to 0$. The above equation is exact, in the case where evaporation-condensation effects are negligible, i.e. when the gas is pushed out of the capillary without offering any mechanical resistance to the advancing liquid. This is not the case for most mesoscopic models available in the literature [7,15], based on a diffusive interface dynamics [19]. As we shall see, only when either the limit of thin interface $\xi/H \to 0$ is reached or when the gas phase density is negligible, $\rho_g/\rho_l \to 0$, the dynamics given by (12) is correctly recovered. Otherwise, deviations induced by condensation/evaporation effects, are observed, which may result in significant departure from the Poiseuille profile inside the gas phase.

4 Numerical results

In a previous paper [21], we pointed out the effects of finite-density jumps, interface width and inertia in LB

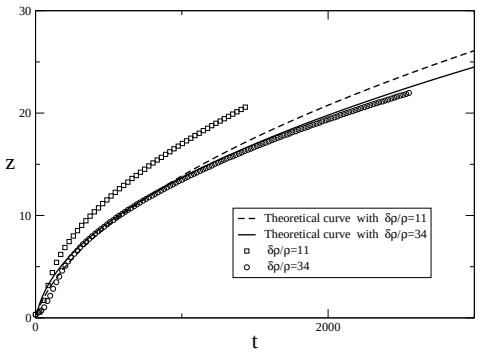

Fig. 2. Evolution of the front coordinate, $z(t)$, for two values of the density ratio, $\rho_l/\rho_g = 34$ and $\rho_l/\rho_g = 11$. For the sake of comparison, the numerical solution of the generalized Washburn equation with the same value of ρ_l/ρ_g is also reported. The figure clearly shows that only the case $\rho_l/\rho_g = 34$ provides good agreement between the two.

simulations of capillary filling. In the present work, we keep focus on the details of the former alone, leaving a more complete discussion to a future and lengthier publication.

4.1 Finite-density effects

In Figure 2 we show the front trajectory $z(t)$ for a given resolution $H = 121$ and two different density ratios, $\rho_l/\rho_g = 11$, $(G = 5.0)$, $\rho_l/\rho_g = 34$, $(G = 6.0)$. The LB solution is compared against numerical solution of the generalized Washburn equation (12). From this figure, it is clearly appreciated that the Washburn solution is quantitatively reproduced only for density ratios above 30.

It is instructive to inspect the internal structure of the flow (Fig. 3). In the left panel, the expected Poiseuille flow is clearly visible for both liquid and gas phases. Of course, distortions from such asymptotic behaviour take place in the vicinity of the moving interface, but since the vapour phase is light enough, such distortions are rapidly reabsorbed away from the interface. As the vapour phase is made heavier, however, such reabsorption no longer takes place, and a *qualitative* change is observed in the flow pattern, with a clear emergence of a 'anti-Poiseuille' flow in the gas phase. Such anti-Poiseuille flow appears to be a direct consequence of the fact that, within this parameter regime, the front evolves under the combined effect of two distinct mechanism: capillary drive *and* front-condensation. The extent to which such condensation holds in real experiments, remains an open issue at this point, and one to which LB can hopefully contribute useful insights for the future. Here, we only wish to offer a few remarks. First, we observe that since front condensation proceeds diffusively, it contributes the same $t^{1/2}$ scaling exponent as capillary advection. This explains why one can recover the correct 1/2 Washburn exponent, and yet miss the right prefactor. This is relevant to LB, since it is known that LB simulations are affected by spurious currents due to lack of isotropy of the higher-order kinetic moments.

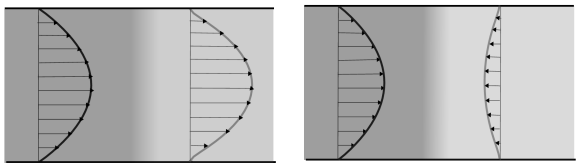

Fig. 3. Streamwise velocity field for the case $\rho_l/\rho_g = 11$ (left) and $\rho_l/\rho_g = 34$ (right).The dark region marks the dense phase.

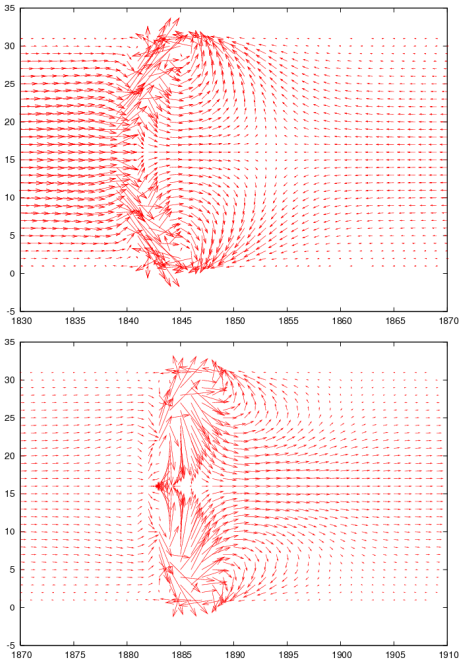

Fig. 4. Two-dimensional velocity pattern for the case $\rho_l/\rho_g = 11$ (upper fig.)and $\rho_l/\rho_g = 34$ (lower fig.). The presence of two rolls (vortices) near the solid wall, ahead and past the front is clearly visible. Equally visible, is in the upper figure, the inverted flow in the light phase, far ahead of the front. The far-field velocity ahead of the front of the lower figure, however, recovers the Poiseuille profile.

One might argue that the rolls shown in figures 4, are just a discreteness artifact due to spurious currents. We are reasonably confident that this is *not* the case, because the same phenomenon has been observed in independent LB simulations using the momentum-conserving free-energy formulation, which is known to suffer less severe spurious-current effects [20]. Moreover, by running the same case at doubled resolution, the same picture has been obtained, namely the vortex intensity was found to stay nearly unchanged. Since it is know that spurious currents decay with grid resolution [9], this provides further confidence that front condensation is a real physical ef-

fect which may occur in experiments near the liquid-gas phase-transition. However, since in LB simulations the interface width is far thicker than in actual experiments, it is possible that the condensation effects predicted by the simulation might significantly overestimate the real ones. It would therefore be desirable to develop a theoretical model to predict the share of condensation/capillarity as a function of the liquid-gas density ratio, possibly by extending the generalized Washburn equation along the ideas outlined in [22]. Work along these lines, as well as to understand the role of dynamic versus static contact angle and additional dissipative effects induced by the front deformation during propagation, is currently underway.

5 Conclusions

The present study shows that Lattice Boltzmann models with pseudo-potential energy interactions are capable of reproducing the basic features of capillary filling, as described within a (generalized) Washburn approximation. Two conditions for quantitative agreement have been identified in the recent past: i) a sufficiently high density contrast between the dense/light phase, $\rho_l/\rho_g > 10$ and a sufficiently thin interface, $\xi/H < 0.1$. In this paper we have focused on the former effect, and shown that at sufficiently high vapour density (above 1/10 of the liquid density) front motion proceeds through a concurrent combination of capillary advection and front condensation. The latter is sustained by an inverted Poiseulle motion in the light phase, providing a steady supply of vapour to the front location, where condensation takes place. Independent LB simulations, based on a different LB formulation, do confirm the same picture, thereby lending weight to the hypothesis that at finite vapour density, capillary filling may proceed through a combination of surface tension drive and condensation. It is also observed that since both mechanisms feature the same scaling exponent, such an hypothesis can only be tested through a detailed and quantitative analysis of the prefactors and not just the exponents. Our data suggest that motion by condensation proceeds faster than the capillary one. Should this indication receive experimental confirmation, one might devise ways of accelerating capillary filling by performing experiments near the critical point.

6 Acknowledgments

Valuable discussions with B. Andreotti, D. Kwok, D. Palmieri, D. Pisignano, G. Ruocco and J. Yeomans are kindly acknowledged. Work performed under the EC contract NMP3-CT-2006-031980 (INFLUS). SS wishes to acknowledge support from the Killam Foundation at the University of Calgary.

References

1. E.W. Washburn, Phys. Rev. **17** (1921) 273.
2. R. Lucas, Kooloid-Z **23** (1918) 15.
3. P.G. de Gennes, Rev. Mod. Phys. **57** (1985) 827.
4. E.B. Dussan, Ann. Rev. Fluid Mech. **11** (1979) 11.
5. L.J. Yang, T.J. Yao and Y.C. Tai, J. Micromech. Microeng. **14** (2004) 220.
6. N.R. Tas et al., Appl. Phys. Lett. **85** (2004) 3274.
7. X. Shan and H. Chen, Phys. Rev E. **47** (1993) 1815.
8. R. Benzi, L. Biferale, M. Sbragaglia, S. Succi and F. Toschi, Phys. Rev. E **74** (2006) 021509.
9. M. Sbragaglia, R. Benzi, L. Biferale, S. Succi, K. Sugiyama and F. Toschi, Phys. Rev. E **75** (2007) 026702.
10. P. Raiskinmaki, A. Shakib-Manesh, A. Jasberg, A. Koponen, J. Merikoski and J. Timonen, J. Stat. Phys. **107** (2002) 143.
11. D. Wolf-Gladrow, *Lattice-Gas Cellular Automata And Lattice Boltzmann Models* (Springer, New York, 2000)
12. S. Succi, *The lattice Boltzmann Equation*, Oxford Science (2001).
13. R. Benzi, S. Succi, M. Vergassola, Phys. Rep., 222, 145, 1992.
14. R. Benzi, L. Biferale, M. Sbragaglia, S. Succi, and F. Toschi, Jour. Fluid Mech. **548**, (2006) 257.
15. A. J. Briant, A. J. Wagner, and J. M. Yeomans, Phys. Rev. E **69**, (2004) 031602.
16. C.H. Bosanquet, Philos. Mag. **45** (1923) 525.
17. G. Cavaccini, V. Pianese, A. Jannelli, S. Iacono and R. Fazio, Lecture Series Comp. Comput. Sci. **7** (2006) 66.
18. J. Szkeley, A.W. Neumann and Y.K. Chuang, J. Colloid Interf. Sci. **69** (1979) 486.
19. D. Jacqmin, Jour. Fluid Mech. **402** (2000) 57.
20. A. J. Briant and J. Yeomans et al, in preparation
21. L. Biferale et al, Europ. J. of Fluids, submitted
22. Y. Pomeau, Self-Assembly, Pattern Formation and Growth Phenomena in Nano-Systems, Springer Verlag, 159-166, 2006.